Mestrado Integrado em Engenharia Química

Sealing of Dye-Sensitized Solar Cells

Master Thesis

by

Rute Marisa Rego dos Santos

Performed at

Faculdade de Engenharia da Universidade do Porto

Supervisor: **Professor Adélio Mendes**

Co-Supervisor: **Doutora Luísa Andrade**

U.PORTO
FEUP FACULDADE DE ENGENHARIA
UNIVERSIDADE DO PORTO

Departamento de Engenharia Química

July 2013

Acknowledgements

I would like to thank my supervisor Professor Adélio Mendes, and my co-supervisor Dr. Luisa Andrade, for the opportunity given to me, for always being optimistic about all the experimental results and especially for the time spent in discussions and all the help provided in the correction of this work.

I would like to thank Fernando Ribeiro and Isabel Mesquita for the experimental help in the laboratory and for all the patience and availability.

I am very grateful to all my friends for their support, love and for the good times we spent together. Thank you Pedro for your support, friendship, patience and availability, kindness... Thank you Jotinha and especially thank you Cris for having been there for me….

Last but not least I would like to thank my family for supporting me during this time.

Abstract

Dye-sensitized solar cells (DSCs) are simple devices able to convert sunlight into electricity. DSCs are constituted by an electrode coated with a nanoporous TiO_2 film sensitized by a dye, an electrolyte containing a redox couple system and a counter electrode coated with platinum catalyst. The simplicity of processing and low cost manufacturing place this technology as a promising alternative to conventional photovoltaic cells based on silicon. Besides having a very efficient device for converting sunlight into electricity, the long-term stability is also a very important requirement for all solar technologies. In particular for DSCs, stability is directly related to the sealing process of the cells.

The present work has as main goal the optimization of assembly Z-type and W-type modules with a voltage of 5 V using a newly developed laser sealing method. Besides, it was also necessary to optimize the scribing of transparent conductive oxide (TCO) thin film for the two types of modules studied. DSCs are applied to glass substrates; these substrates are coated by a TCO layer, usually fluorine doped tin oxide, for driving photogenerated electrons to the external contacts. Thus, in a module- configuration, scribing of the TCO is needed for allowing electrons generated in a cell to be conducted to the adjacent cell. For Z-type modules, the flow of electrons occurs from a substrate to another. Thus, it is necessary to use a conductive material in contact with both substrates – a kind of “elevators” - capable of transferring the generated electrons. Therefore, several materials were tested and characterized to assess their ability of being used in DSCs devices as “elevators”.

Resumo

As células solares sensibilizadas por corante (DSCs) são dispositivos simples capazes de converter a luz solar em eletricidade. As DSCs são constituídas por um elétrodo revestido com um filme nanoporoso de TiO_2 sensibilizado por um corante, um eletrólito que contém um par redox adequado e um contra- elétrodo revestido com um catalisador de platina. A simplicidade de processamento e o baixo custo de fabrico fazem com que esta tecnologia se apresente como uma alternativa promissora às células convencionais à base de silício. A estabilidade a longo prazo é um requisito básico, de todas as tecnologias solares. No caso particular das DCSs, a estabilidade está diretamente relacionada com processo de selagem das células.

O presente trabalho tem como principal objetivo a otimização do processo de montagem de módulos do tipo Z e tipo W com uma diferença de potencial de 5 V utilizando o método de selagem a laser recentemente desenvolvida. Tendo em vista o objetivo principal apresentado, foi necessária também a otimização do corte do filme do óxido condutor transparente (TCO) para os dois tipos de módulos estudados. As DSCs são produzidas em substratos de vidro. Estes substratos são revestidos por uma camada de TCO, geralmente óxido de estanho dopado com flúor, que permite a condução dos eletrões fotogerados para os contactos externos. Assim, numa configuração do módulo, o corte/scribing do TCO é necessária para permitir que os eletrões gerados numa célula possam ser conduzidos para a célula adjacente. Para os módulos de tipo Z, o fluxo de eletrões ocorre de um substrato para outro. Assim, é necessária a utilização de um material condutor em contacto com ambos os substratos - uma espécie de "elevadores" - capaz de transferir os eletrões gerados. Neste contexto, vários materiais foram testados e caracterizados para avaliar a sua capacidade de serem utilizados em dispositivos DSCs como "elevadores".

Declaration

I declare, on oath, that this work is original and that all the not original contributions are appropriately identified with the respective source.

Porto, 31st July 2013

(Rute Marisa Rêgo dos Santos)

Index

Figures Index

Tables Index

Glossary

Variables	Definition	Units
E_C	Conduction band energy	J
E_g	Bandgap energy	J
E_{Redox}	Redox energy of the electrolyte	J
E_v	Valence band energy	J
J_{MPP}	Current density in the maximum-power point	$mA \cdot cm^{-2}$
I_S	Incident light intensity	$mW \cdot cm^{-2}$
J_{SC}	Short-circuit current density	$mA \cdot cm^{-2}$
V_{MPP}	Voltage in the maximum-power point	V
V_{OC}	Open-circuit voltage	V

Abbreviation	Definition
AM	Air mass
CB	Conduction band
CE	Counter electrode
DSCs	Dye-sensitized Solar Cells
e^-	Electrons
FF	Fill factor
FTO	Fluorine doped tin oxide
ITO	Indium tin oxide
MPP	Maximum-power point
PV	Photovoltaic
S	Ground state of the sensitizer

S^*	Excited state of the sensitizer
S^+	Oxidised state of the sensitizer
TBA	Tetrabutylammonium
TBP	Ter-butylpyridine
TCO	Transparent conductive oxide
UV	Ultraviolet
VB	Valence band
WE	Working electrode

1 Introduction

Presently large amounts of fossil fuels are still consumed to produce energy but there is a widespread concern of society with the environment leading to an emerging demand for clean and inexhaustible energy. Moreover, the high dependence on non-renewable energy of the last hundred years has also strongly contributed to a major problem – the global warming. Global Warming is caused mainly due to anthropogenic activities associated with the burning of fossil fuels, leading to the emission of greenhouse gases such as CO_2, CO, NO_x and CH_4.[1, 2] These gases, in the atmosphere, absorb some of the radiation emitted by the earth causing the greenhouse effect, thus increasing the average temperature of the planet. Since replacing all fossil fuels is still an impossible task, the solution is to mitigate these gases by developing new technologies that can be used to produce energy from renewable sources.

In this context, solar energy arises as one of the most appealing renewable energy due to its inexhaustible and freely available source - the sun. The average rate of energy consumption in 2000 was 13 TW and it is expected to reach 28 TW in 2050. The amount of energy that comes from the sun and strikes earth is 1.7×10^5 TW; the practical terrestrial global solar potential is assumed to be 600 TW; with the use of cells with an efficiency of about 10 %, the energy produced can reach 60 TW which would be enough to satisfy our current needs.[3-5]

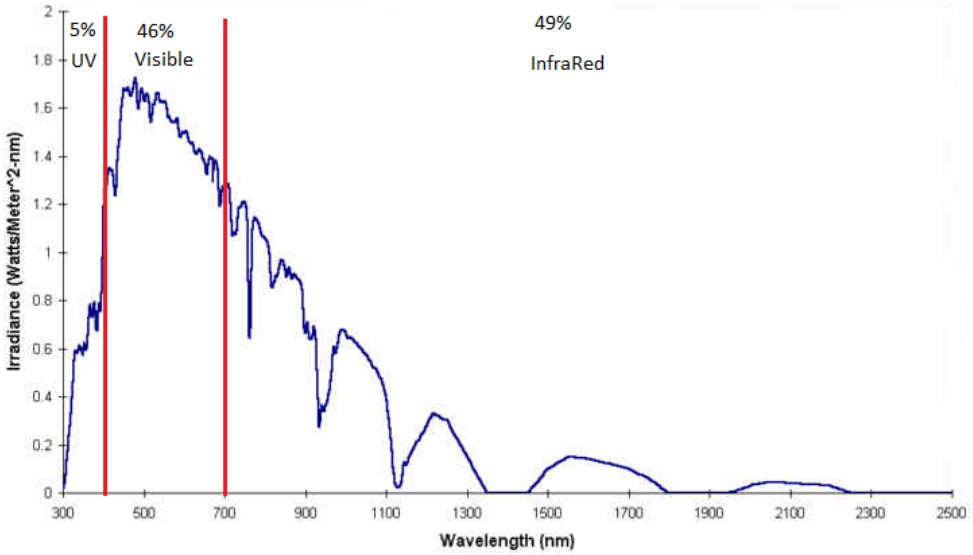

Figure 1 - Solar Spectrum (according to ASTM-G173).

Solar energy has the potential to fulfill an important part of the energy demand of future generations. Dye sensitized solar cells (DSCs) emerged as a cheap technology due its easy and fast fabrication, low production costs and high photoelectric conversion efficiencies.[2, 6-8] However, as for all solar cell technologies, long term stability is a basic requirement. Considering DSC technology, the stability is directly related to the sealing process of the cell.[9, 10] The sealing with conventional materials, such as Surlyn, is very sensitive to temperature and they allow oxygen and humidity to get in contact with the inner-components of the cell, which, over time, strongly contribute to the decrease of efficiency of the cell. Therefore, to prevent this situation, it is necessary to develop a more effective sealing.

1.1 Objectives of this work

In the framework of this work the optimization of assembly Z-type and W-type DSC modules with a voltage of 5 V, using a newly developed laser sealing method, is envisaged. It was also optimized the scribing of the transparent conductive oxide (TCO) layer. DSCs electrodes have as substrates glass; since glass does not conduct electricity, these substrates are coated by a TCO film, usually fluorine doped tin oxide, for driving the photogenerated electrons to the external circuit. Thus, in a module-configuration, scribing/cutting the TCO film is needed for allowing electrons generated in a cell to be conducted to the adjacent cell. Furthermore, in Z-type configuration, the flow of electrons occurs from a substrate to another. Thus, it is necessary to use a conductive material in contact with both substrates capable of transferring the generated electrons. Several materials were also tested and characterized to assess their ability of being used in Z-type modules as appropriate connectors.

1.2 Outline of this thesis

Chapter 1 introduces the scope of this thesis, giving a general overview about the topic and describing the main goals.

In Chapter 2, DSCs' state of the art is overviewed, explaining the working principles of a dye-sensitized solar cell. The organization of single cells in module is also discussed. A special focus is given on the DSC way of operation, characterization of each inner-components and the performance analysis.

Chapter 3 describes the experimental details for producing dye-sensitized solar cells, as well as the laser sealing process. It is further described the process for producing W-type modules, as well as the study of connectors for Z-type modules.

In Chapter 4, the obtained results and the respective discussion are presented. The conclusions of this work are present in Chapter 5. Finally, Chapter 6 describes the main goals achieved, work limitations and suggestions for future work.

2 State of Art

The photovoltaic technology emerged in 1839 when the physicist Alexandre Edmond Becquerel observed the generation of an electric current between two platinum electrodes immersed in an illuminated electrolyte.[11] This was the first observation of the photovoltaic effect, defined as the production of potential or electrical current between two electrodes when one of them is illuminated.[8, 12] Nevertheless, the photovoltaic effect remained for decades as only a scientific phenomenon without any practical application. Only in 1877, the first solar cell based on selenium was built and in 1883 Charles Fritts described this cell in detail; though the efficiency of these devices was very small, less than 1%.[13-15]

The real photovoltaic technological developments began in 1954. Daryl Chapin, Calvin Fuller and Gerald Pearson from *Bell Telephone Laboratories*, USA, developed the first silicon solar cell device using a diffused silicon p-n junction, with an efficiency of 6 %.[12, 16, 17] This value of efficiency was increased to 14 % in 1960 mainly due to the work developed by *Hoffman Electronics* Company. *Bell Telephone Laboratories* presented the first silicon module in October 1955*; t*his first application of solar cells was conducted in Georgia to feed a local telephone network.

In the 1960 decade the development of photovoltaic technologies was mainly for space applications. The *Vangard I* was the first satellite with solar cells. This satellite was launched to space in 1958 carrying a small solar panel. However, in the 70's, due to oil crisis, the cells production for terrestrial applications increased. In fact, this crisis boosted the search and development of technologies that produce energy from renewable sources as photovoltaic technology.[12, 18-20]

Many researches contributed to improve solar cells based on silicon, called the first generation solar cells. These solar cells have high production costs and moderate efficiency. The development of thin film solar cells represented the second generation solar cells and allowed to overcome some of the problems of the first generation solar cells. Second generation of solar cells offered lower costs and more efficiency. The third generation of solar cells arises to improve the efficiency of second generation thin-film technologies.[12, 19, 21-23] Organic cells and DSCs are representative of this new generation.

Organic cells use polymers as semiconductors. This type of cells has the advantage of being flexible with low costs. However, these cells have low efficiencies and severe degradation pathways since the exposure to sunlight degrades the organic material.[24]

DSCs, also known as Grätzel solar cells, were developed for the first time by Michael Grätzel in 1991. While in conventional cells the function of semiconductor is to absorb the light and conduct generated charges to the load, in DSCs these functions are separated: the dye absorbs sunlight, photogenerates electrons in a high energy level and the semiconductor conducts these electrons to the external circuit. [12, 25, 26] Dye sensitized solar cells have been extensively studied. This type of cells provides a technically and economically credible alternative concept, due to their potentially low cost of production and relatively high energy conversion efficiency, currently ~14 %. For a DSC module the efficiency is about 9.9 %, achieved by Sony, Japan.[2, 6-8, 12, 25, 26]

2.1 Dye – Sensitized Solar Cells

DSCs have been considered one of the candidates for the next generation solar cells. These cells are constituted by a oxide semiconductor, a sensitizer (dye), an electrolyte, a catalyst and conducting glass as substrates. A schematic presentation of DSC is show in Figure 2.

2.1.1 Working Principles of a DSC

A DSC is a simple device but its working principles are very different of conventional solar systems, wherein the semiconductor simultaneously absorbs the light and carry the photogenerated charges to the load; in DSCs these two functions are separated. The light is absorbed by a sensitizer (dye) which is attached to the surface of the semiconductor. The charge separation is performed at the interface semiconductor/electrolyte.

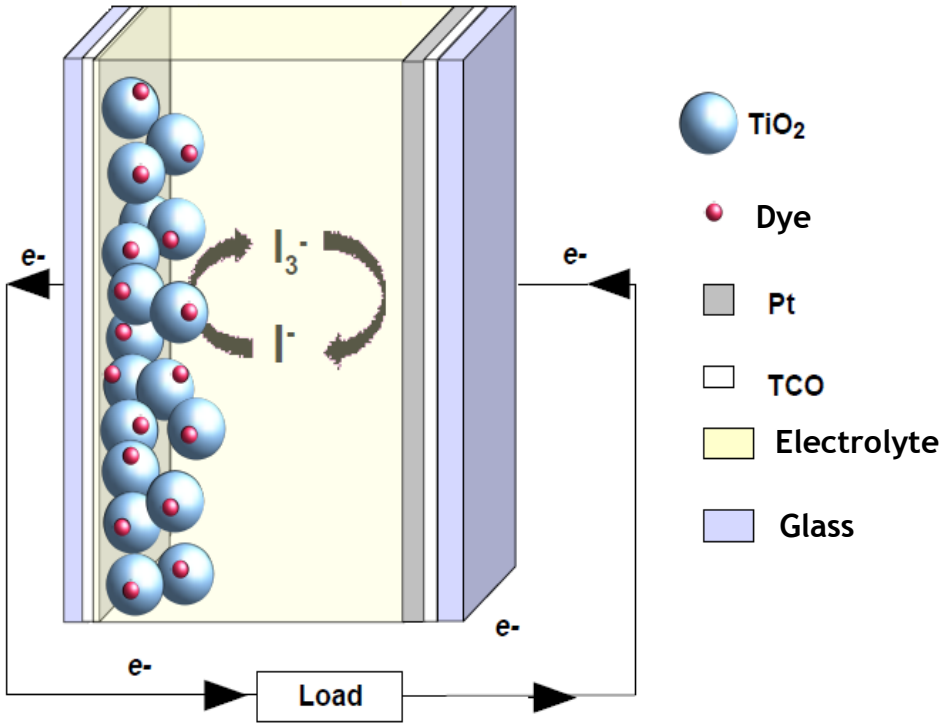

Figure 2 - Schematic representation of a dye sensitized solar cell.

The photoelectrode, also known as working electrode (WE), is typically composed by a mesoporous layer of titanium dioxide (TiO_2) covered with a dye monolayer. Platinum (Pt) is used as counter electrode of the cell. Between the two electrodes is the electrolyte, which contains a redox couple (I^-/I_3^-). The photoelectrode and the counter electrode are deposited in glass substrates coated with a thin transparent conductive oxide film (TCO).

DSCs working principles can be compared to photosynthesis, where chlorophyll in green leaves absorbs sunlight. When a photon is absorbed, an electron is photoexcited from ground state to an excited state into the dye molecule. Then, electron injection from the excited state dye into the TiO_2 conduction band occurs. After that, electrons migrate by diffusion through the TiO_2 network, towards the external circuit, and come back to the cell through the counter electrode. In the counter electrode, reduction of redox couple occurs at its surface, catalyzed by platinum. The original state of the dye needs to be restored to allow millions and millions of turnovers. Thus the oxidized dye molecule is regenerated by accepting electrons from iodide ions; triiodide ions are produced and they diffuse back to the counter-electrode to be reduced back to iodide by electrons from the external circuit. This process closes the cycle.

Figure 3 shows the operating principles of a DSC.

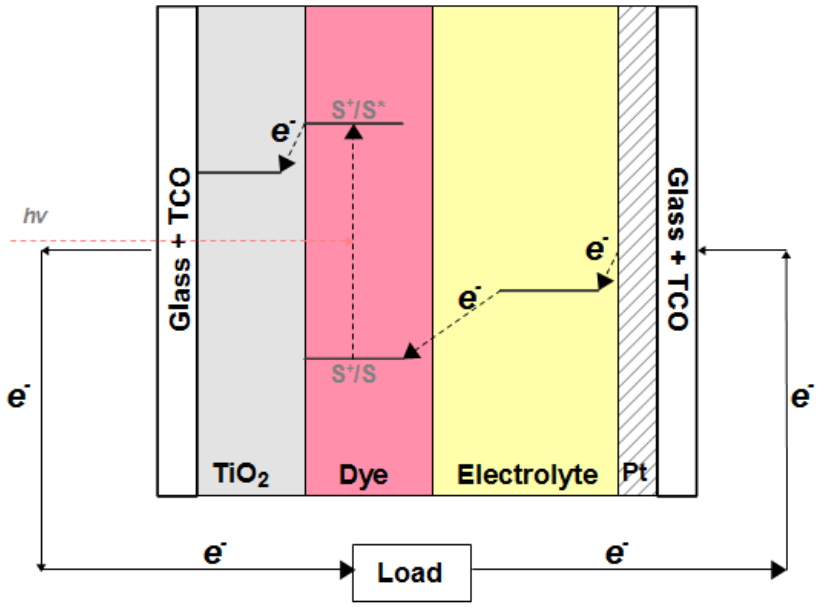

Figure 3 - Schematic energy diagram and operating principle of DSC.

A step by step explanation of the DSC operating principles is presented below:

1. Incident light is absorbed by the photosensitizer (S), which is anchored to the surface of the semiconductor. The photosensitizer is excited from the ground state (S) to the excited state (S^*):

$$\mathrm{S} + hv \rightarrow S^* \tag{1.1}$$

2. The excited electrons are injected into the conduction band of the TiO_2 electrode, resulting in the oxidation of the photosensitizer (S^+).

$$\mathrm{S}^* \rightarrow \mathrm{S}^+ + \mathrm{e}^-_{\mathrm{CB_{TiO_2}}} \tag{1.2}$$

3. The oxidized photosensitizer (S^+) accepts electrons from the I^- ion redox mediator, regenerating the ground state (S), and I^- is oxidized to the oxidized state, I_3^-.

$$S^+ + \frac{3}{2}\mathrm{I}^- \rightarrow \frac{1}{2}\mathrm{I}_3^- + S \tag{1.3}$$

4. Injected electrons in the conduction band of TiO_2 flow through the semiconductor to arrive at the back contact (TCO) and consequently through

the external circuit to the counter electrode. The oxidized redox mediator, I_3^-, diffuses toward the counter electrode and is reduced to I^- ions.

$$I_3^- + 2e^- \rightarrow 3I^- \quad (1.4)$$

Additionally, some undesirable reactions resulting in losses in the cell efficiency occur, such as:

5. Dye excited-state can decay to ground state without injection of electrons in conduction band of TiO_2:

$$S^* \rightarrow S \quad (1.5)$$

6. Recombination of the injected electrons with oxidized sensitizer:

$$S^+ + e^-_{CB_{TiO2}} \rightarrow S \quad (1.6)$$

7. Recombination of the oxidized couple at the TiO_2 surface:

$$I_3^- + 2e^-_{CB_{TiO2}} \rightarrow 3I^- \quad (1.7)$$

The most important loss mechanism is the recombination of TiO_2 conduction band electrons with triiodide ions in the electrolyte – reaction 1.7. Thus, it is important to realize that the triiodide concentration in DSC must be small. However, this concentration must be high enough to promote the reduction of triiodide ions on the counter-electrode by platinum.

2.1.2 Characterization of the components of a dye-sensitized solar cell

Semiconductor

Semiconductors have an empty conduction band (CB) while the valence band (VB) is completely filled by electrons (Figure 4a). Between these bands there is an energy gap called bandgap. When the energy supplied is greater than the bandgap of the semiconductor, an electron is promoted from the valence band to the conduction band, leaving a hole in the valence band (Figure 4b).

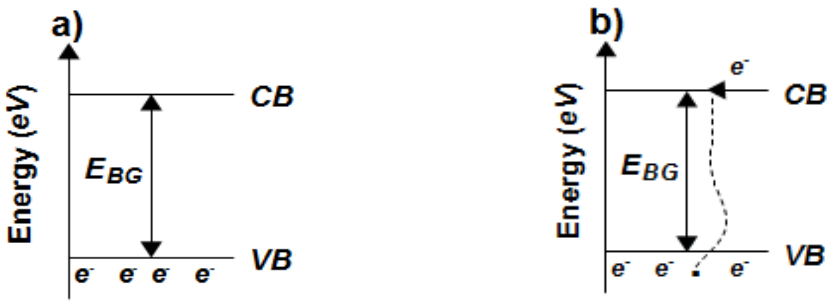

Figure 4 - Energy diagram of the semiconductor.

The most used semiconductor in DSCs devices is the titanium dioxide. Other semiconductor oxide films have been studied for the same application, such as ZnO, SnO_2, Nb_2O_5, CeO_2 and $SrTiO_3$, however, TiO_2 is the one that presents the best results for DSC.[3, 27] The function of TiO_2 in a DSC is to give support to the dye, being also collector and load conductor. TiO_2 is a transparent semiconductor which is not sensitive to visible light ($\lambda = 420nm$), non-toxic, with a high index of refraction, chemically inert and cheap.[3, 28-30]

Titanium dioxide exists in three crystal structures: rutile (tetragonal), brookite (orthorhombic) and anatase (tetragonal). The rutile is mainly used by the pigments industry due to its optical efficiency (opacity and whiteness) and durability. The anatase structure is a semiconductor with a bandgap energy of 3.2 V.[3, 27, 31, 32] The *CB* of TiO_2 remains slightly below the conduction band of the dye, allowing an efficient injection of electrons.

Characteristics such as the surface area and the porosity of the film are important. The high surface area of TiO_2 improves light absorption since a higher amount of dye can be adsorbed on TiO2 surface. The porosity is important because the electrolyte, which contains redox ions, must be able to penetrate the TiO_2 film, to allow the dye regeneration (reaction 1.3). TiO_2 films are deposited on a conductive glass substrate by "doctor-blading" or "screen-printing" techniques. Typically, these films have, on average, a thickness of 8 – 12 *μm*.

Dye

The semiconductor is coated with a photosensitizing dye. The dye is sensible to visible light. Thus, it collects light of visible wavelengths and subsequently injects photoexcited electrons into the conduction band of the semiconductor. The excited state level of the dye should be higher in energy than the conduction band edge of the semiconductor, to allow an efficient electron injection.[3] An ideal sensitizer for

dye-sensitized solar cells should fulfil some essential characteristics, such as: absorbing a wide range of radiation (400-920 nm), fast injection of electrons in the conduction band of TiO_2 and high stability in order to allow redox cycles.[3, 30, 33, 34]

The dyes used in DSC are divided into two types: organic dyes and inorganic dyes. The latter include metal complexes, such as polypyridyl and complexes of ruthenium (Ru) while organic dyes include natural and synthetic organic dyes. Usually, the dye is a metal complex based on ruthenium component due to their high stability, outstanding redox properties and good response to natural sunlight. Most well-known Ru complexes for DSC are *N3*, *N719*, *N749* and *Z907*. *N3* absorbs up to 800 nm. *N719* dye has the same structure as *N3* dye but has TBA^+ (tetrabutylammonium) instead of H^+ at two carboxyl groups. *N749* dye, which is called black dye, has achieved the maximum absorption up to 860 nm and showed performance similar to N3 and N719 dyes. However, the absorption coefficient of *N749* is lower than *N3* and *N719* dyes. As a result, more efforts have been made to synthesize new dyes with high photon absorption coefficients.[3, 30, 33, 35, 36] Figure 5 shows the molecular structure of the most common dyes, *N719* and *N3*.

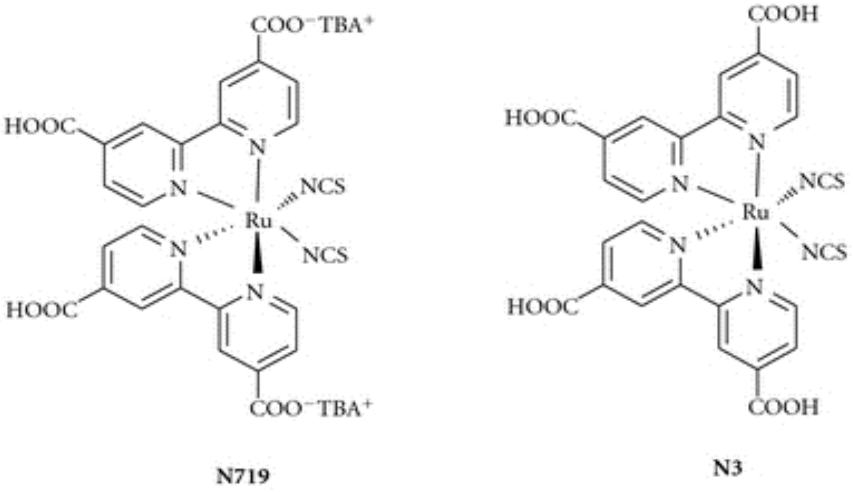

Figure 5 Molecular structures of N719 and N3.[37]

The organic dyes have advantages compared to the inorganic dyes. They are cheaper and non-toxic. However, they have lower efficiency. Much research has been developed in order to improve/modify this type of dyes. The improvement/modification of dyes is one of the essential strategies to improve the performance of DSC.[3, 30, 33-35]

Electrolyte

Since the beginning of the development of DSCs, the electrolyte with a redox couple I^-/I_3^- in an organic solvent is widely used. The thermal stability, high diffusion coefficient and suitable viscosity are some of the features that electrolytes must have. The redox couple must also present some features such as a good solubility and high ion mobility in an organic solvent to ensure high concentration of charge carriers in the electrolyte.[38-40]

The function of the electrolyte is to transfer electrons from the counter electrode to the oxidized dye, which is anchored to the surface of the semiconductor – regeneration of the dye.[36, 38, 40-42] The redox couple I^-/I_3^- has been widely used in DSCs due to its favourable recombination kinetics: the electron donation by I^- is sufficiently fast for efficient regeneration of the dye, while the reduction of I_3^- at the counter-electrode is slow enough to allow high carrier collection efficiencies.[33]

The main disadvantage of the electrolyte currently used is its volatility. The highest efficiency of DSC was obtained based on this type of electrolytes since they have an efficient infiltration in nanocrystalline films but many alternative redox systems such as Br^-/Br_3^-, $SCN^-/(SCN)_3^-$ and-SeCN/$(SeCN)_3^-$, Co^{2+}/Co^{3+} and organic systems are being investigated. Ionic liquids are also presented as a good alternative since they have characteristics that include a suitable viscosity, they are very conductive and have excellent thermal stability and they are not volatile. However, the high viscosity translates to a low mobility of ions (low diffusion coefficient).[43]

More recently, cobalt redox couples were found to give surprisingly high efficiencies in combination with the donor-π-bridge-acceptor (D-π-A) sensitizers. The efficiency observed for this system was 11.9 %. The conjugation of the porphyrin dye with the cobalt dye gives an excellent photovoltage of almost 1 V and an enhanced final photocurrent of more than 17 $mA \cdot cm^{-2}$. This occurs since the molecular design of the dye decreases the interfacial back reaction between excited electrons in the TiO_2 conduction band and the cobalt ions in the redox mediator. Moreover, this dye has an enhanced visible spectrum absorption, which increases the final photocurrent of the system. This was further improved by adding a co-sensitizer, resulting in a record efficiency of 12.3 %.[44]

Counter Electrode

The reduction of triiodide to iodide occurs at the counter electrode. The presence of a catalyst is necessary for the reaction (reaction 1.4) to occur quickly. Typically, the platinum catalyst is used due to its high conductivity, electrocatalytic

activity, stability and its transparency. Nevertheless, the high cost and dissolution of platinum in corrosive electrolytes makes it necessary to search for alternatives.

High surface area, high conductivity, chemical stability and low-cost are some requirements for counter-electrodes in DSC. Carbon materials (active carbon[45], carbon nanotubes[46, 47], graphene[48-50], carbon black[51], etc), conductive polymers[52, 53] and other materials has shown to be an efficient alternative. However, the efficiency of these DSCs in most cases is inferior to that of DSCs with a Pt-based CE.

2.1.3 Sealing of DSC

The sealing material should be thermally stable and chemically inert to the redox couple contained in the electrolyte. For larger area applications, such as solar modules, the sealing material must also protect the conductor and prevent mass transport between the electrolytes of neighbouring cells.[10]

The most common methods for sealing DSCS use polymers such as Surlyn or Bynel. However, a long-term stability is required and the sealing with these polymers originates fast aging of the device. The thermo-compressive glass frit bonding process (Figure 6) is an interesting method due to its thermal and mechanical stability, adding to the fact that it is chemically inert for the electrolyte and for any conductive metal grid. However, this sealing method also requires high temperatures and some mechanical pressure, compromising the dye stability.[9, 10, 54, 55]

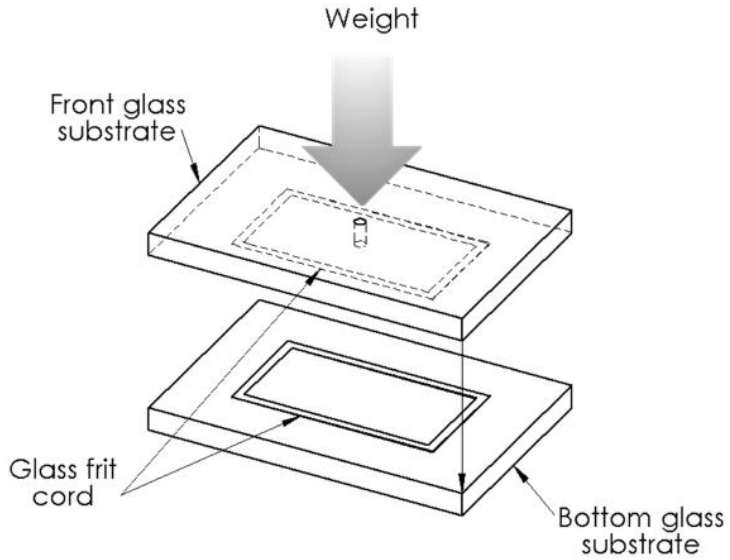

Figure 6 - Schematic representation of the thermo-compressive glass frit bonding process.[55]

Laser - assisted glass frit sealing process emerges as an alternative to the sealing processes mentioned above. The laser beam is fired to the sample and locally

heats the glass paste cord to its melting point (Figure 7), i.e. only the glass paste is subjected to high temperatures, preventing damages in commonly used materials in the photoelectrode and counter-electrode. It is necessary to heat the sample, because it reduces the thermal shock between the laser and the glass substrates, thus preventing the cell damage.[54, 55]

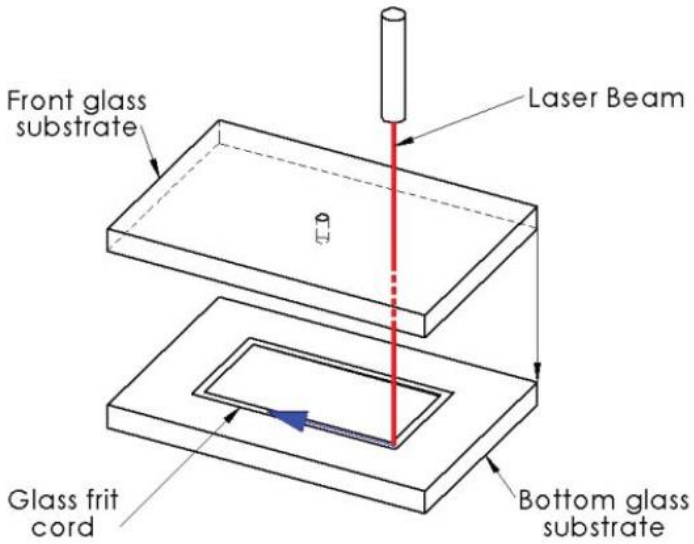

Figure 7 - Schematic representation of the laser-assisted glass frit bonding process.[55]

2.1.4 - DSC analysis performance

The most often tool used to characterize a DSC is based on the characteristic curve current-voltage (*I-V*) (Figure 8), from which the solar cell energy conversion efficiency (η), under full sunlight irradiation, can be determined (Equation 1.8).

2.1.4.1 I-V characteristics of a solar cell

Through the analysis of the *I-V* curve the main electrical characteristics of a cell are obtained: short-circuit current density (J_{SC}), open-circuit voltage (V_{OC}), maximum power point (*MPP)* and Fill Factor (*FF*).

$$\eta(\%) = \frac{J_{SC} \times V_{OC} \times FF}{I_0} \times 100\% \qquad (1.8)$$

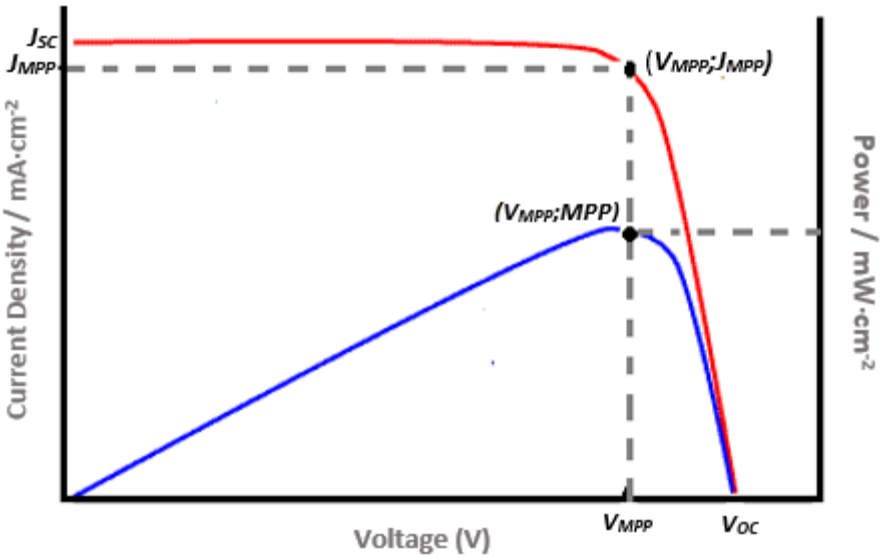

Figure 8 - Typical I-V curve of a solar cell (red line) and respective power curve (blue line) to estimate the relationship (Equation 1.9) of the open circuit voltage (V_{OC}), short-circuit current (J_{SC}), fill factor (FF), and photoelectric conversion (η), where MPP denotes the maximum point of output.

The parameter fill factor reflects the deviation of the *I-V* curve from the ideal characteristic curve. It is defined as the maximum power divided by the product of J_{SC} and V_{OC} according to Equation 1.9:

$$FF = \frac{J_{MPP} \times V_{MPP}}{J_{SC} \times V_{OC}} \qquad (1.9)$$

where, J_{MPP} (mA·cm^{-2}) and V_{MPP} (V) are the current density and voltage at the maximum power output, respectively.

The efficiency of a solar cell is highly dependent on the incident irradiation I_0. Typically, and for comparison reasons, the solar cells are characterized at light intensity of AM 1.5 global - 100 mW·cm^{-2} or 1000 W·m^{-2} (I_0). This light intensity is also referred to as 1 sun.

2.2 Modules of Dye Sensitized Solar Cells

Envisaging the up-scaling of this solar technology, individual cells have to be connected into modules. Individual cells connected in series have to be assembled

into modules to deliver a high usable voltage, a simplified processing pathway, low cost-efficiency, good aesthetic and appearance - Figure 9.

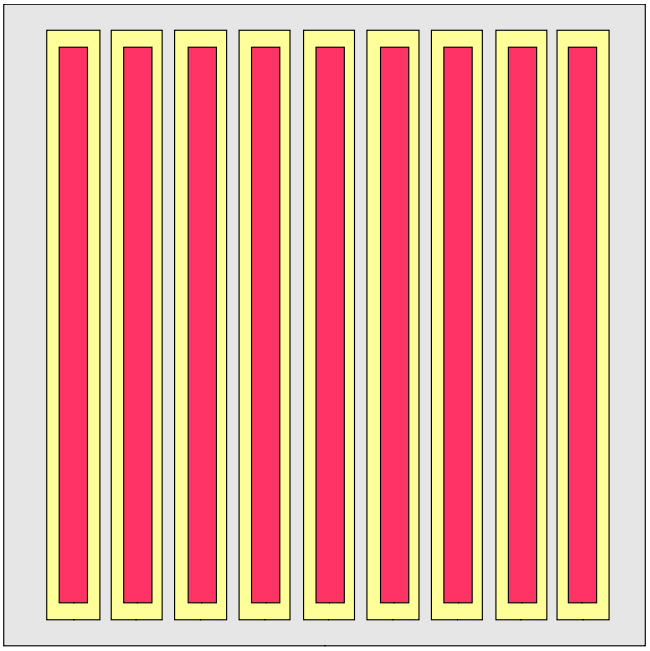

Figure 9 - Sketch of a module - individual cells connected in series.

2.2.1 Type of DSC modules

This integrated series connection for DSC modules can be designed in two ways: Z-type and W-type modules. To promote the conduction of the electrons according to the type of module it is necessary to cut TCO film.

Z - type Modules

In Z-type modules the photoelectrodes of all individual cells are printed in the glass substrate and all the counter-electrodes in another one - Figure 10. In order to allow the flow of current through the different individual cells without having short-circuit it is needed a TCO cutting (red lines) and an interconnection between neighbouring cells provided by a conductor medium. Therefore, the electrons will be conducted through the "connector", from the photo-electrode of one cell to the counter electrode of the neighbour cell.

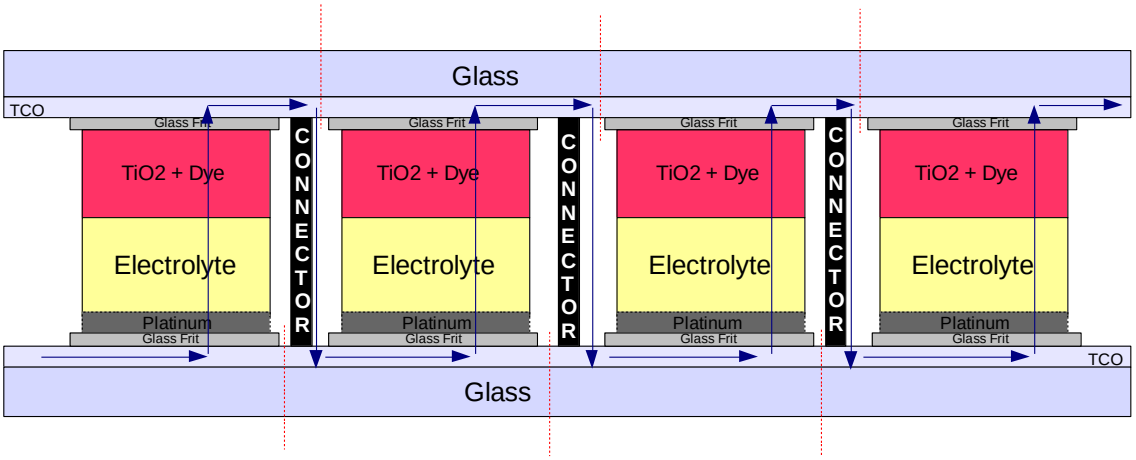

Figure 10 - Modules assembled with a Z-configuration. The blue arrows indicate the electrons flow.

W – type Modules

In W-type modules, the photo- and counter-electrodes are placed on the same substrate alternately, as seen on Figure 11. W-type modules need a cut in TCO (red lines) in order to avoid the flow of electrons from the counter-electrode to the photo-electrode of the neighbour cell. Thus, the electrons are conducted from the counter-electrode to photo-electrode of the same cell.

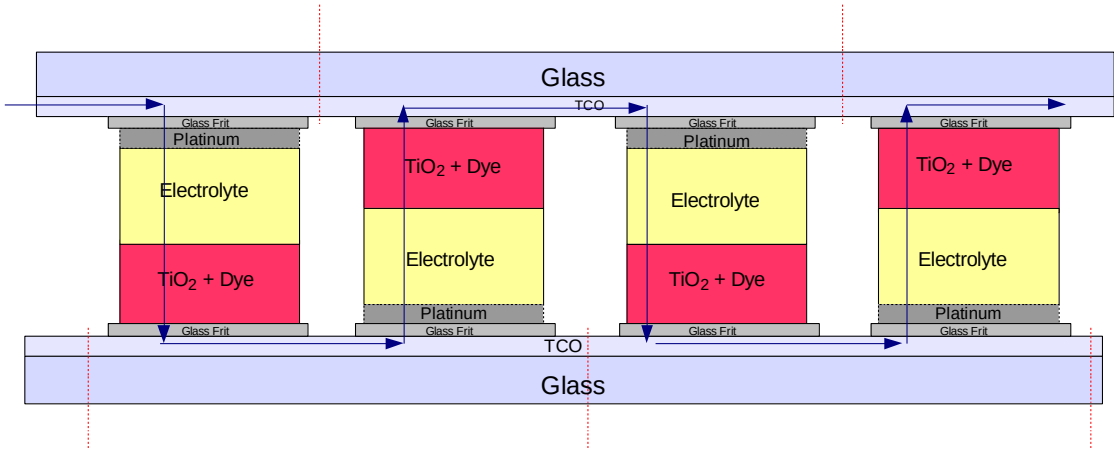

Figure 11 - Modules assembled with a W-configuration. The blue arrows indicate the electrons flow.

TCO scribing

Thin transparent conducting oxides films on glass substrates, such as fluorine doped tin oxide (FTO) or indium tin oxide (ITO), are extremely common materials used as the current collector for thin-film photovoltaic (PV) devices. The laser scribing process is used to remove the conductive oxide film, i.e., to make a cut in TCO allowing connection of cells in series.

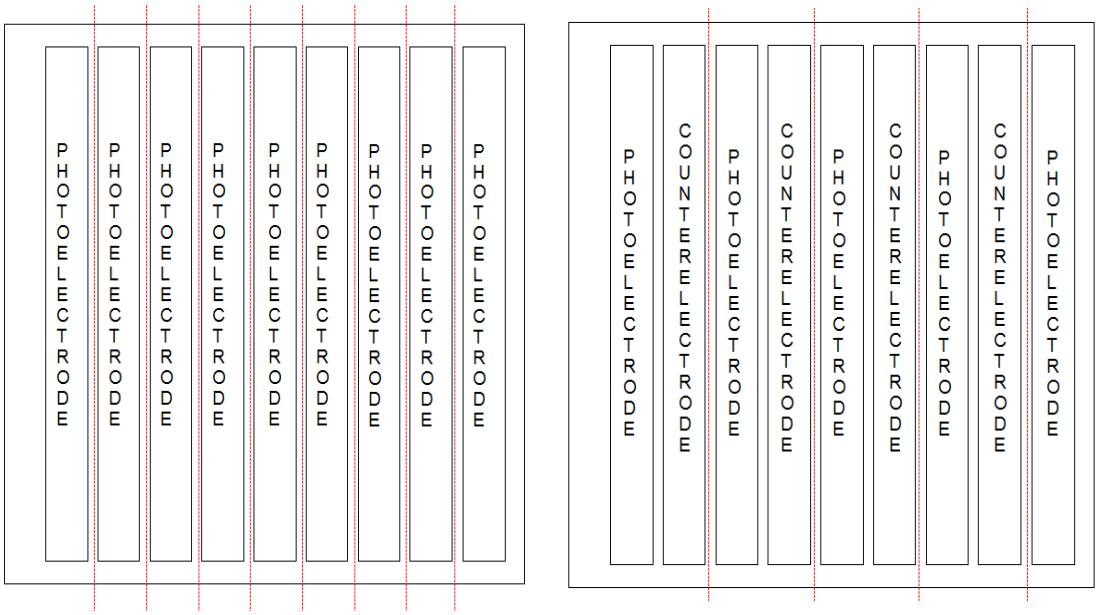

Figure 12 - TCO scribing in Z-type and W-type modules, respectively.

In Figure 12 a TCO cutting in Z-type modules is represented. The cut in the TCO layer is made among all the cells of the module (red line). As regards to W-type modules, represented, the cut in TCO layer is made between each two cells (red line).

2.2.2 Modules analysis performance

The characterization of a DSC module is made similarly to the characterization of individual DSCs. Through the *I-V* curve the same parameters are obtained - V_{OC}, J_{SC}, *FF*, *MMP* - allowing the determination of the module's efficiency. The only difference in module characterisation is that the *Voc* of the module is the sum of the *Voc* of all the individual cells. This is actually the reason why cells are assembled into modules.

3 Procedure and Technical Description

In this chapter, the process of assembling a dye sensitized solar cell and a dye sensitized solar module is described in detail. The optimization of TCO cutting and the study of suitable elevators are also assessed.

3.1 Material

To assemble a DSC device it is needed the following materials: the conductive glass (TCO22-7) soda-lime based and coated with fluorine doped tin dioxide (SnO_2: F or FTO), the dye (N719 Ruthenizer 535 bis-TBA), the semiconductor (TiO2-Nanoxide T/SP) and the catalyst (Platisol TSP); all the materials are bought to the company Solaronix (Switzerland). The glass paste used is a mixture of a lead-free glass frit ceramic particles with organic solvents and binders.

3.2 DSC assembling

The assembly of a DSC involves several steps, starting with the TCO glass preparation: i) glass marking and cutting (size of 20 × 10 × 2 mm conductive glasses), ii) making the holes on counter-electrode, iii) washing and UV treatment of the glass. Then follows the printing and sintering steps of the printable materials: the glass paste cord, and the platinum counter-electrode and the TiO_2 paste in the respective glass substrates. The photoelectrode glass is placed on top of the counter-electrode g.lass and both substrates are laser sealed. This is followed by dye recirculation, electrolyte filling and the sealing of the holes. Each step will be further described below.

3.2.1 Glass treatment

The glass treatment considers marking, cutting and washing. The marking of the glass with TCO was done on *VersaLaser* equipment and it was made on the TCO side. The holes in the glass were made using a *DREMEL* machine with a cylindrical diamond drill; the glass was immersed in a container with water. The holes are made in the counter-electrode glass substrate.

The glass cleaning includes the use of two devices: washing system *Amsonic* and *UV* cleaning system. The *Amsonic* consists of three tanks and a drying chamber. The first tank contains distilled water with detergent at a temperature of 55 °C, the second and the third contained only distilled water at room temperature. After washing, the glass is placed in the drying chamber, at 60 ºC for 20 minutes. The UV treatment used to remove organic compounds that may remain on the surface of the glass even after washing; the glass is subjected to this treatment for 15 minutes. This cleaning step of the glasses is of crucial importance since it will determine the good adhesion of the inner-components to the respective substrates.

3.2.2 Electrodes preparation

A screen printer (*ROKUPrint 2.2)* was used to print the semiconductor, the sealing material and the platinum catalyst of the DSCs; each component uses a different screen material. After printing the pastes, they are sintered in accordance to the temperature profiles shown in Figure 13. Sintering the electrodes removes all of the solvent and binders from the components of DSCs.

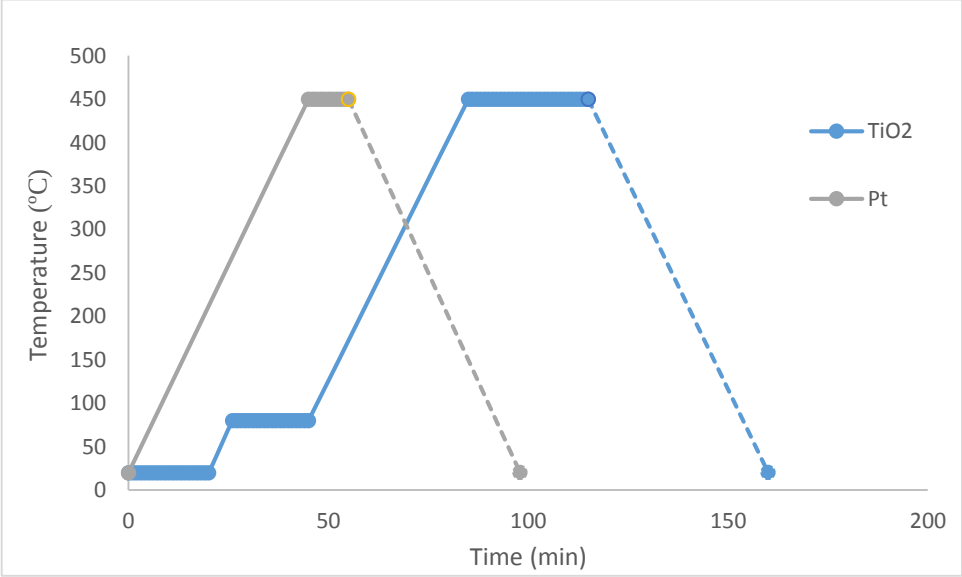

Figure 13 - Sintering profile of titanium dioxide, platinum and glass paste.

The glass paste is the first component to be printed. Before printing the glass paste it has to be homogenized on a mixer mill using zirconium oxide grinding jars with zirconium oxide balls, for 50 min. This is a very important step: a bad printing of this material directly interferes with the success of the laser sealing process.

3.2.3 Sealing of the cell

The photoelectrode substrate should be carefully placed over the counter-electrode glass substrate and slightly pressed. The next step was to transfer the sandwich cells to the *LaserBox* equipment and place them on the controlled heating plate. The heating of the cell is done gradually, i.e., a heating rate of 5 °C/min was applied in order to avoid the formation of internal tensions in the substrates. Finally, the laser assisted sealing was performed. Important to mention that after placing the sandwich cells in the LaserBox, it is necessary to align the glass paste cord with the pointer of the laser beam. This was possible with the help of the guideline, controlled by a *Labview software*. When the alignment was finished, the guidelines were aligned with the glass paste.

3.2.4 Dye Recirculation and Electrolyte Filling

The dye recirculation was done by injecting a solution of N719 dye on one of the holes of the counter-electrode. Through the second hole, the dye was collected for reprocessing - Figure 14. The recirculation was performed, on each cell, for 12 hours.

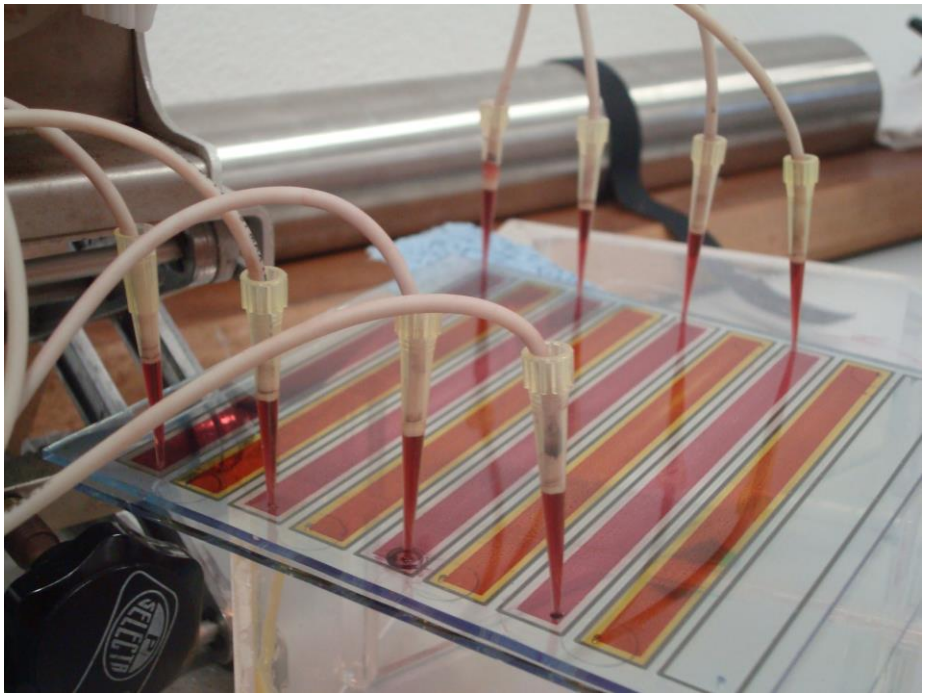

Figure 14 - Dye recirculation.

After staining, the TiO_2 layer was washed with pure solvent (ethanol) to remove unabsorbed dye molecules and dried under nitrogen.

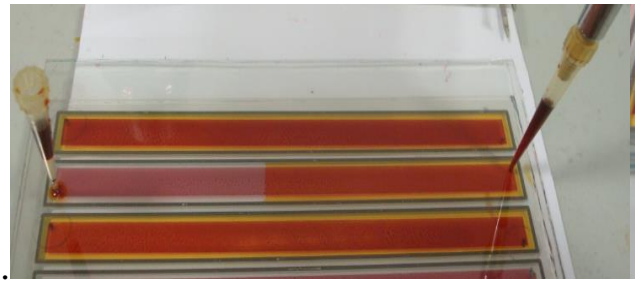

Figure 15 -Electrolyte Filling.

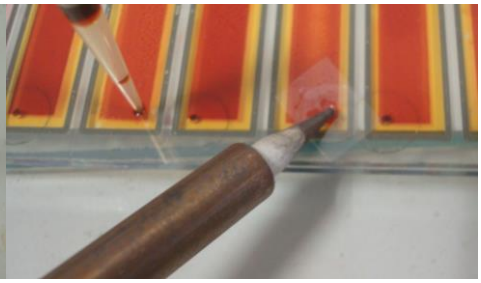

Figure 16 - Holes Sealing.

Electrolyte filling was done through a micropipette as shown on Figure 15. Finally, the holes on the counter-electrode were sealed with Coverslip Glass - Figure 16.

3.2.5 Performance analysis

The performance analysis of the modules was made on a solar simulator *KW Large Area Light Source* (*Newport 92193-1000)*, with a Xenon Lamp (*Newport 1600W Xenon Ozone Free*) and a *Power supply* (*Newport 69922*). Data acquisition was made using an electrochemical workstation from *Autolab (PGSTAT302N by Echo Chemie)* and the computer software used to treat the data was *NOVA 1.9*. Based on the obtained data, the *I-V* curve of the module can be obtained and thereafter the characteristic parameters short-circuit current density, open-circuit voltage, maximum power point and fill factor.

3.3 DSC module assembling

As described before, individual cells are connected in series in a module configuration to allow a higher voltage of the final device. Nevertheless, the electrons pathway through the different cells has to be well defined in order to avoid short-circuit within the cells of the module. This means that this pathway has to be drawn by TCO cutting. Thus, the optimization of the TCO scribing was also performed. W-type modules of 150 × 150 × 20 mm^3 were built. In the case of Z-type module, the connectors were also chose and tested.

3.3.1 Optimization of the TCO scribing

The optimization of the TCO scribing was performed on the equipment *VersaLaser* with a laser able to cut TCO films. This process was optimized through the variation of different parameters such as power, speed and number of pulses per inch (PPI) of the laser. The results were then evaluated using a magnification camera (*CB-080GE Camera Ethernet with a lens Zoom 70XL with internal focus, Jai CB-080GE*). The thickness of the cut was measured using a software tool (*ImageJ*) through the comparison with the thickness of a graphite mine.

3.3.2 W - Type Module

After printing and sintering the glass paste, the layer of TCO on the glass substrate was structured by laser scribing to determine the desirable electron pathway. The cleaning process was repeated to remove possible glass residues of the TCO cutting. Then, the TiO_2 layer and the platinum layer were screen printed on the respective substrates. After sintering, the counter and photo electrode were aligned and subsequently laser sealed.

3.3.3 Z – Type Module: Connectors optimization

The Z-type modules need metal connectors to drive electrons from one glass substrate to the other. This implies a more complex processing procedure than W-type modules but more efficient devices. Before starting preparing Z-modules, adequate connectors should be selected. These connectors should have the following features: high conductivity; should resist to the sealing temperature without changing their properties; and after the sintering process they should present a thickness similar to the one of the glass paste cord that is connecting the two substrates. The selected connectors to test for DSCs applications were: a typical silver paste for photovoltaic connectors (SP 1248), two types of polymer silver pastes from *Ferro* (LF 7122 and LF 7123), three tin welds (Sn99.3Cu0.7, Sn60Pb40 and S-Sn63Pb37) and a copper tape.

To test the different connector's materials, mini-modules of 40× 25 × 2 mm were assembled mimicking all the processes of a large module - Figure 17. Thus, the glass paste was printed, in this case by "doctor-blading" for simplicity, and then sintered according to the conditions shown in Table 1. After this, the TCO was cut

and the glass washed to eliminate any residues. The connectors are placed as shown in Figure 17 and then the mini-module was sealed as described before. Nevertheless, depending on the type of material used, they may need a sintering process before sealing. Indeed, the silver pastes were sintered accordingly to Table 1, while tin welds and copper tape need no sintering process; it is the temperature achieved during the sealing step that induces the adhesion between the conductive material and the substrates.

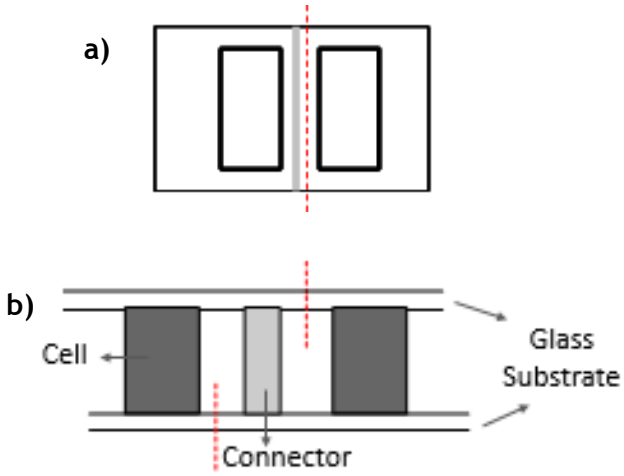

Figure 17 -a) Schematic representation of mini-module, with TCO cut (red line) and connector (grey line); b) side view.

Table 1 - Printing and sintering conditions.

	Silver paste		
	LF 7122	**LF 7123**	**SP 1248**
Thickness / mm	0.13 0.19	0.13 0.19	0.13 0.19
Glass Paste Print	One side	One side	One side
Sintering Temp / °C	200	200	475
Sintering Time / min	10	10	30

Regarding tin welds and copper tape, the tests were performed at three different sealing temperatures, 250 °C, 300 °C and 370 °C. These temperatures were chosen taking into account the limit of the melting point of each material. The welding tests for these materials were more difficult to accomplish because the welds have a cylindrical structure, making it difficult to align with the substrates. The welds were polished to remove the varnish and to make them less cylindrical.

4 Results and Discussion

In this chapter it is presented the main results obtained in the framework of the present work developed for assembling dye-sensitized solar cells and dye sensitized solar modules laser sealed. The optimization of the TCO cut and the study of suitable elevators (connectors) for Z-Type modules is also assessed.

4.1 Surlyn Sealing *vs*. Laser Sealing

Figure 18 presents the *I-V* curve for two DSCs sealed by different methods: Surlyn sealing and laser-assisted sealing.

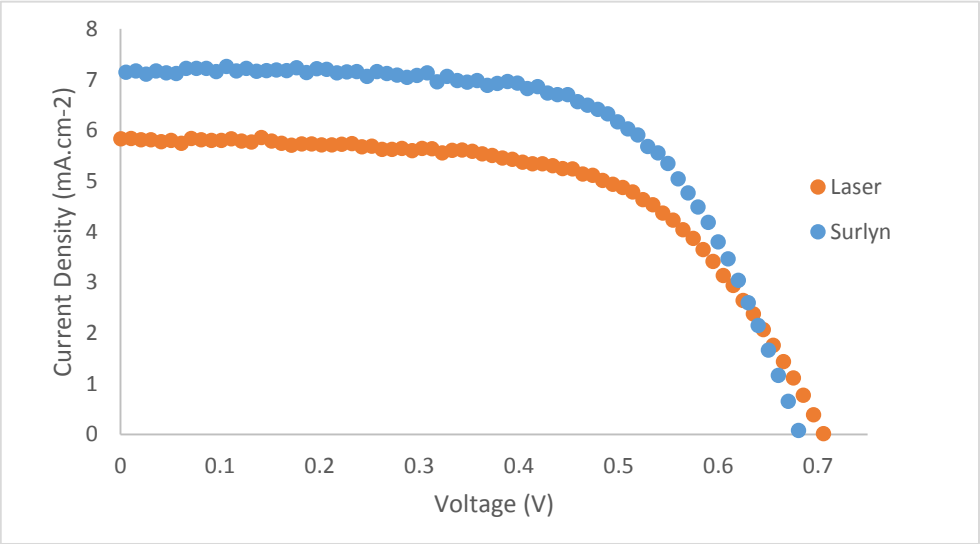

Figure 18 - I-V curve.

In Table 2 the operating conditions and the correspondent efficiency results of the individual cells sealed by different processes are presented.

Table 2 - Sealing conditions and results.

	Surlyn	***Laser***
Active area /cm^{-2}	0.2	0.8
***Voc* / V**	0.68	0.71
***Jsc* / mA·cm^{-2}**	7.2	5.8
***Is* / mW·cm^{-2}**	100	100
MPP / mW·cm^{-2}	3.1	2.5
FF	0.63	0.59
Efficiency (%)	3.1	2.5

The efficiency of the cell sealed by laser technique is slightly lower. However, this difference results from a larger active area of the cell laser sealed. Thus, it can be concluded that the sealing laser technique is a good alternative to conventional sealing. In fact, the sealing procedures should not interfere with the efficiency of the devices but only with stability.

4.2 Modules – Laser Sealing

The laser sealing technique applied to DSC modules was optimized. For that, several glass-glass substrates were sealed without inner-components inside - Figure 19 - to determine the correct parameters of sealing - Table 3.

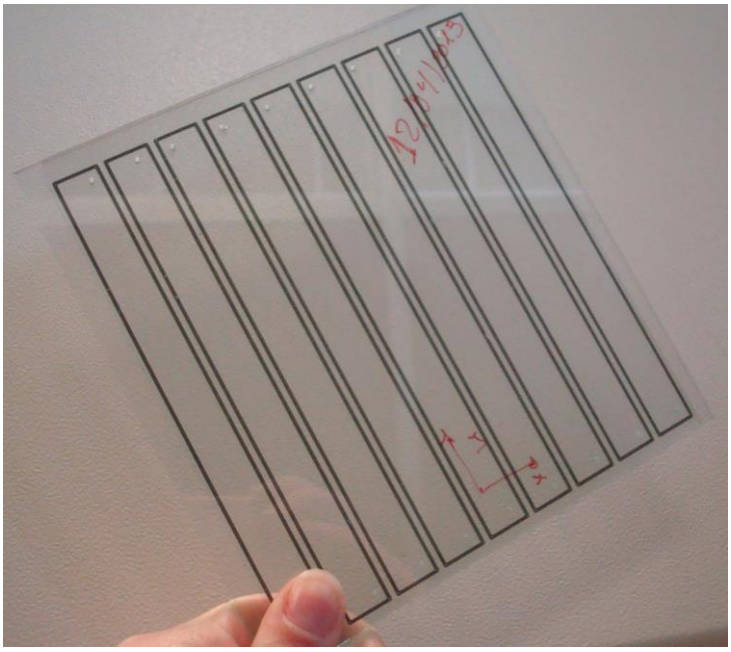

Figure 19 - Sealed glass-glass module.

Table 3 - Sealing parameters for W-type modules.

	Sealing parameters for cells 150x150x2mm	
Laser Power	23%	
Optical gain	xx: 1.361	yy: 1.342

A difference exists between the pointer and the spot where the laser fires. This difference corresponds to the difference between what the operator sees, when the aligning is being made, and where the laser effectively focuses. Thus, the optical gain can vary according the operator. This is being now improved by incorporating a

robotic arm and a camera to allow this alignment to be completely automatic. This new process will greatly increase the reproducibility of the sealing. The temperature and the optical gain are the most important parameters regarding a successful laser sealing.

Depending on the type of modules that are being sealed, the electrons should flow as indicated by the red arrows represented on Figures 20 and 21. This is only possible by cutting the TCO, as mentioned before.

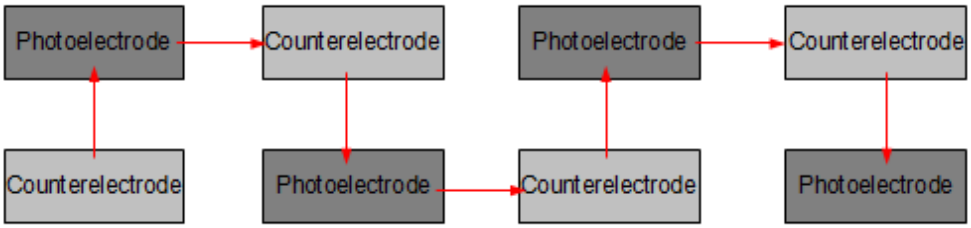

Figure 20 - Schematic representation of flux of electrons on W-type modules.

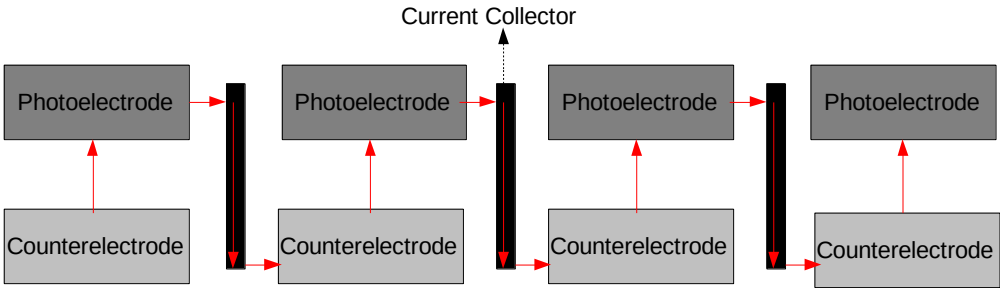

Figure 21 - Schematic representation of flux of electrons on Z-type modules.

The cuttings performed with help of the equipment VersaLaser need to be optimized depending on the type of glass used and also to ensure that the TCO thin film is completely interrupted and no current is allowed to flow through. In Figure 22 some test cuts made by laser scribing are shown. Based on these cuts, the correspondent thickness can be assessed and the correspondent optimal parameters of the laser VersaLaser can be then identified - Table 4.

Figure 22 - Scribing tests.

Table 4 - Characteristics of the laser VersaLaser.

Characteristics of Versa LASER	
Power	2 %
Speed	5 %
Pulses per inch (PPI)	1000

The low resistance (close to zero) measured by the multimeter proves that the parameters chosen are appropriate. The analysis of each of the cuts through the camera CB-080GE confirmed that the parameters shown in Table 4, are the most suitable. Through the analysis of each cut, using the *ImageJ* software tool, it was possible to determine the optimal thickness of the cut on the TCO. Figure 23 represents the worst cut and Figure 24 the best one, in this case with thickness of about 0.048 mm.

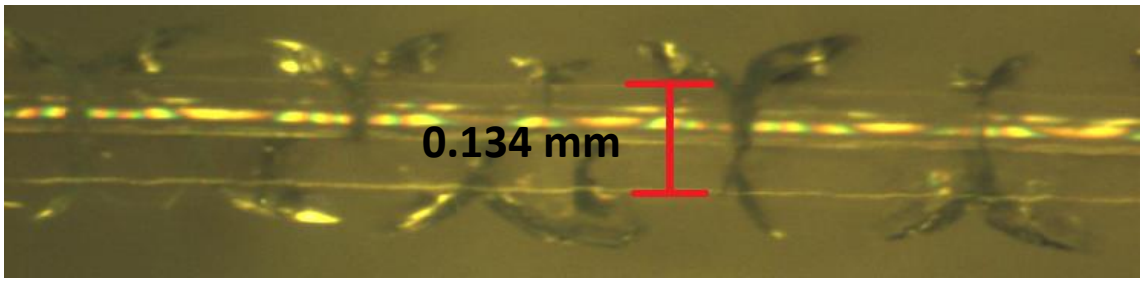

Figure 23 - Laser scribing test - the worst cut.

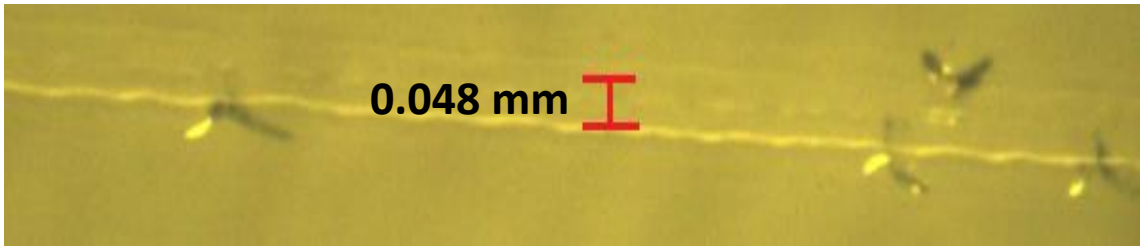

Figure 24 - Laser scribing test - the best cut.

4.3 Laser Sealing of W-type modules

The laser sealing was performed successfully in four W-type modules, as shown in Figure 25.

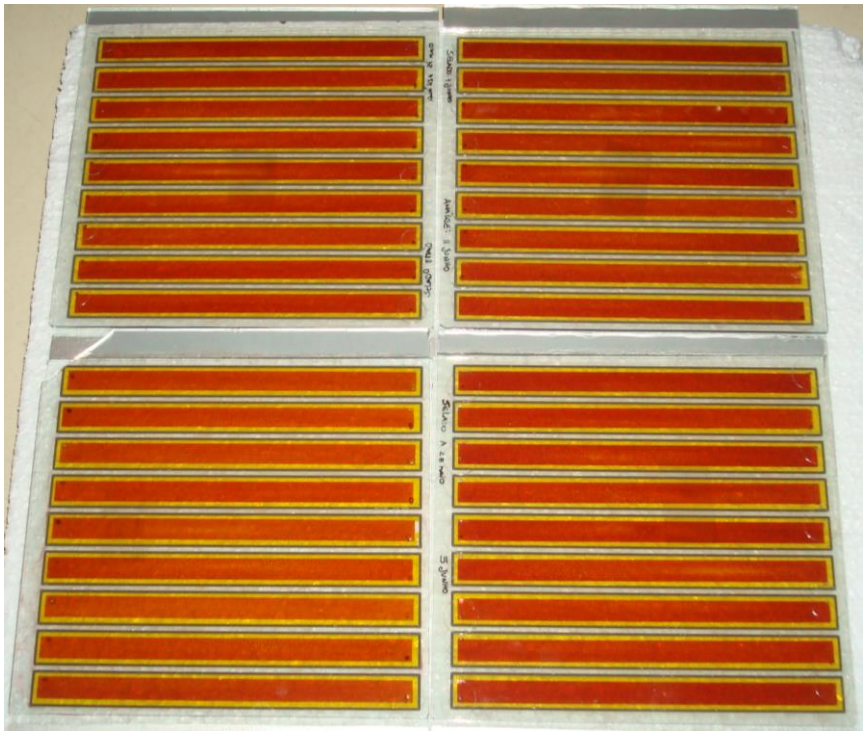

Figure 25 - W-type modules.

Figures 26 and 27 show the *I-V* curves for the four W-type modules assembled. In the W-type modules, the photo and counter-electrodes were placed on the same substrate alternately. Thus, Figure 26 corresponds to the *I-V* curve of four photoelectrodes illuminated (front illuminated), while figure 27 represents five photoelectrodes illuminated (back illuminated). Through the analysis of the *I-V* curve the main electrical characteristics of each module were obtained: short-circuit current density (J_{SC}), open-circuit voltage (V_{OC}), maximum power point (*MPP*) and fill factor (*FF*) - Table 5 and Table 6, respectively.

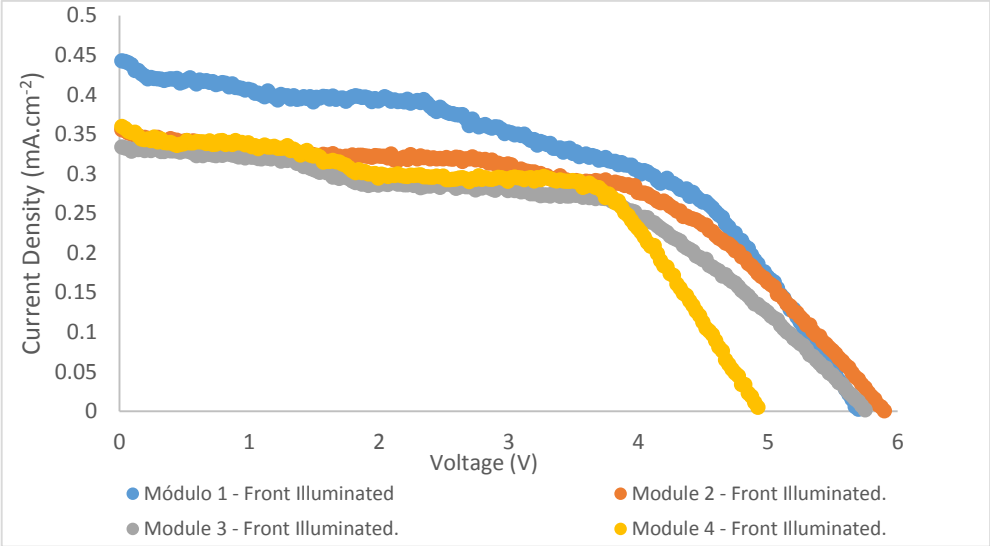

Figure 26 - I-V curve for front illuminated modules.

Table 5 - Results for front illuminated modules.

	Module 1	***Module 2***	***Module 3***	***Module 4***
Active Area /cm²	99.1	99.1	99.1	99.1
Voc / V	5.71	5.91	5.76	4.93
Jsc / mA·cm⁻²	0.45	0.36	0.34	0.36
Is	99.4	99.4	99.4	99.4
MPP / *mA·cm⁻²*	1.24	1.13	1.01	1.05
FF	0.49	0.53	0.53	0.59
Efficiency (%)	1.25	1.14	1.02	1.05

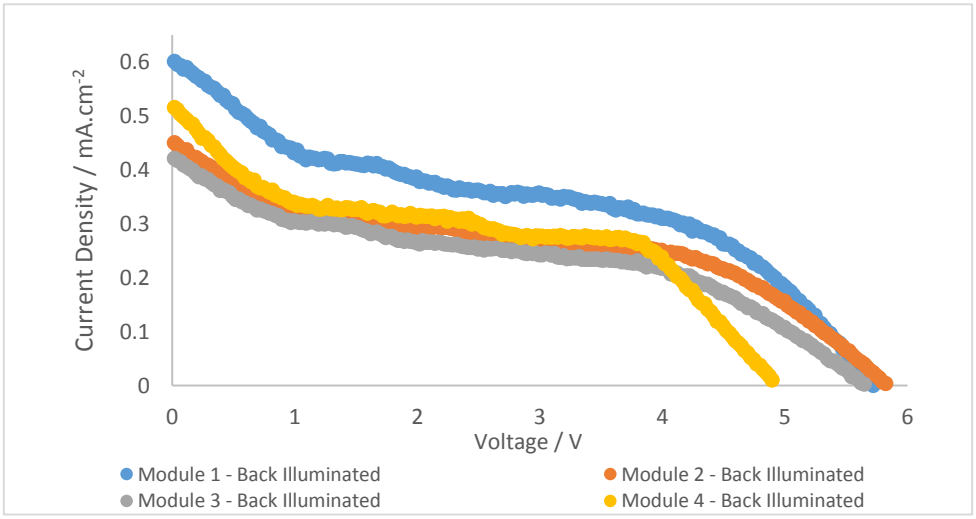

Figure 27 - I-V curve for back illuminated modules.

Table 6 - Results for back illuminated modules.

	Module 1	***Module 2***	***Module 3***	***Module 4***
Active Area / cm^2	99.1	99.1	99.1	99.1
Voc / V	5.73	5.83	5.66	4.91
Jsc /$mA \cdot cm^{-2}$	0.61	0.45	0.43	0.52
Is	99.4	99.4	99.4	99.4
MPP / $mW \cdot cm^{-2}$	1.26	1.01	0.88	1.02
FF	0.36	0.38	0.36	0.40
Efficiency (%)	1.27	1.02	0.88	1.03

In all the modules tested, it was expected a higher efficiency for the back illuminated when compared with the front illuminated. However, this is not the case. As we can see in Table 7, the associated experimental errors may explain this inconsistency of results.

Table 7 - Mean values of modules efficiency and it's associated standard deviations.

	Average	***Standard Deviation***
Front Illuminated	1.12	0.104
Back Illuminated	1.05	0.162

4.4 Connectors to Z-type modules

It was also expected to validate the assembling of Z-type modules but due to time limitations it was only possible to optimize the connectors/elevators used in this configuration. Considering the connectors tested and described in section 3.3.3, Table 8 shows the electrical resistance results for silver pastes before and after sealing and Table 8 refers to the tests concerning three tin welds and a copper tape. The melting point of the silver pastes are unknown and only the sintering temperatures are given in the respective datasheets. In the case of silver paste SP 1248, the sintering temperature is quite high, ca. 475 °C, what means that the melting point is even higher and so the optimum sealing temperature can be used for this paste. Regarding the silver pastes LF 7122 and LF 7123, the sintering temperature was 210 °C, which does not guarantee that the melting temperature is higher than the sealing temperature. Thus, analyzes were performed, with gradual increase in temperature, to check the stability of the material, until it reaches 370 °C. It was observed that at this temperature the silver paste is not melted yet.

Figure 28 - Mini-modules with silver paste 7122, 7123 and SP 1248, respectively.

Table 8 - Silver paste resistivity characteristics.

Test Conditions	***Silver paste***		
	LF 7122	**LF 7123**	**SP 1248**
Initial paste resistance / Ω	0.001	0.001	0.001
Sealing temp / ºC	370	370	370
Print paste	one side	one side	one side
Thickness / mm – Test 1	0.13	0.13	0.13
Electrical resistance after sealing / Ω	0.38	0.41	0.36
Thickness / mm – Test 2	0.19	0.19	0.19
Electrical resistance after sealing / Ω	0.39	0.27	0.39

The electrical resistance of the analyzed silver pastes was measured with a multimeter after being sandwiched in a module configuration. For the thinner silver connector:

$$SP\ 1248 < LF\ 7122 < LF\ 7123$$

While, for the thicker sample it was found that:

$$LF\ 7123 < SP\ 1248 = LF\ 7122$$

The values of the electrical resistance measured are inconclusive since the obtained values are not that different. Nevertheless they may indicate that the polymeric silver pastes from *Ferro* are more appropriate for these applications.

Regarding the tin welds and copper tape tests, their melting points are known. As the theoretical melting point of each of the welds is lower than the sealing temperature, it was necessary to test these welds at different temperatures to verify their behaviour.

The welds in Figures 31 and 32 show the results obtained for the lower and higher temperature, 250 °C and 370 °C, respectively.

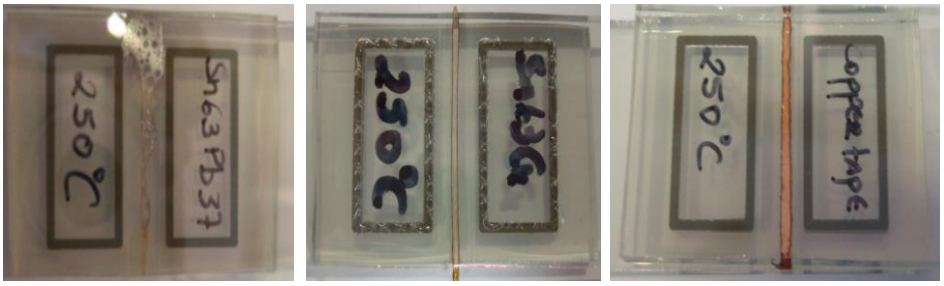

Figure 29 - Tested welds at 250ºC: S-Sn63Pb37, Sn99.3Cu0.7 and copper tape, respectively.

Figure 30 - Tested welds at 370ºC: S-Sn63Pb37, Sn99.3Cu0.7 and copper tape, respectively.

Table 9 shows the measured electrical resistance of these materials at different temperatures. The best performing welds with lower electrical resistance at all tested temperatures are tin welds Sn60Pb40 or S-Sn63Pb37 weld. However, these welds have lead, which makes them not suitable for this type of application. Thus, these results were only used as a comparison. The copper tape showed lower values of resistance at 370 ºC, when compared with weld Sn99.3Cu0.7.

Table 9 - Test Conditions and electrical resistance of the tin welds and copper tape.

Material	*Melting Point / ºC*	*Test Temperature / ºC*	*Electrical Resistance / Ω*
Sn60Pb40	**186**	250	-
		300	0.287
		370	0.218
S-Sn63Pb37	**183**	250	0.289
		300	0.287
		370	0.290
Sn99.3Cu0.7	**227**	250	0.420
		300	0.309
		370	0.301
Copper Tape	**No Data Available**	250	0.306
		300	0.310
		370	0.284

These values are close to the values of resistance measured for the tin welds containing lead, as well as for silver pastes. Thus, the copper tape is an option to be considered as a connector in Z-type modules.

The silver pastes, the tin welds and the copper tape have very similar electrical resistances. However, recent tests suggest that the resistance is controlled by the substrate (TCO) and not by connectors. In order to verify this assessment, additional testing is required.

5 Conclusions of this work

The present work has as its main purpose, the optimization of the assembly of Z-type and W-type modules. To achieve this goal, several steps have been made, since the optimization of the TCO scribing to the study of current collectors for Z-type modules.

Initially, it was programed the assembly of four modules of each type, i.e., W- type and Z- type. However, as the sealing implies the alignment of the glass cord with the pointer of the laser by the operator, it still presents low reproducibility.

The W-type modules were successfully prepared and characterized. The voltage obtained for these modules was of approximately 5 V. Regarding Z-type modules, several tests were conducted using different materials, at different temperatures, in order to determine suitable connectors/elevators to be used in this configuration. These tests allowed to identify that copper tape is a promising material to be used as a connector for Z-type configurations.

6 Evaluation of work undertaken

6.1 Goals achieved

The main objectives of the work developed in the framework of this master thesis were:

- **Assembling dye-sensitized solar cells modules with the newly developed laser-assisted sealing technique**: a new sealing technique for DSCs was recently developed by the research group in which it was developed this master thesis. Individual cells are already able to be laser sealed with a high reproducible process; it is now of utmost importance to start preparing modules (arrangement of several individual cells connected in series).
- **Study of two different configurations for modules preparation**: two different approaches were followed for assembling DSCs' modules: W-type and Z-type. The two configurations differ in terms of the process complexity, efficiency and cost.
- **TCO optimization**: the modules are formed by several individual cells. The electrons generated in one cell must be conducted to the adjacent cells until they were collected in the external circuit. This means that the electrons have to be conducted by a specific pathway in order to avoid short-circuit of the module. This pathway is delimited by TCO cuts that determine the way electrons must follow. These cuts were studied in terms of thickness and width by optimizing the operating parameters of the scribing equipment.
- **Study of connectors for Z-type modules**: Z- type modules imply the flow of electrons from one glass substrate to the other. This means that between the two glasses substrates it is needed a conductor material in contact with both substrates able to transfer electrons generated in one side to the adjacent one. Several materials were studied: a) silver pastes due to their good conductivity, b) tin welding and copper tape.

6.2 Limitations and future work

In the first part of this work I got familiar with all processes and procedures to prepare individual dye-sensitized solar cells. The process of laser sealing was also used. Then, glass-glass modules were optimized in terms of sealing. Since this step

implies the alignment of the glass cord with the pointer of the laser by the operator, this process is still low reproducible. The biggest challenge in this work was to optimize the sealing parameters of a module of 9 cells with dimension $15 \times 15 \times 2mm$. This goal was successfully reached. Then, it was needed to start with the assembling of complete modules (with photoelectrode, electrolyte and counter-electrode materials). This needs several steps of printing and sintering, very time consuming processes due to the temperature profiles needed to be accomplished. It was decided to start by the W-type configuration since it is less operational complex than Z-type. Thus, four complete W-type DSC modules were successfully prepared and characterized. At this stage is it only missing the optimization Z-type modules. As explained this type of module configuration implies the use of connectors to bring electrons generated in one substrate to the other substrate. Several materials to be used as connectors were tested and characterized. Even though, there were no more time to prepare complete Z-type modules. Since the most promising connector's materials were already identified it is suggested for future work the optimization of the assembling process of Z-type configuration modules. Additionally, the study and optimization of the printing procedures in order to have a better uniformity in the printing step should be also envisaged; actually this was strongly limiting the efficiency of the modules.

7 References

1. Eisenberg, R. G. N., Daniel, Preface: Overview of the Forum on Solar and Renewable Energy. *Inorganic Chemestry* **2005,** 44, (20), 6799-6801.

2. Yanhong, L.; Dongmei, L.; Qingbo, M., Towards Optimization of Materials for Dye-Sensitized Solar Cells. *Advanced Materials* **2009,** 21, 4647-4651.

3. Hagfeldt, A.; Boschloo, G.; Sun, L.; Kloo, L.; Pettersson, H., Dye-sensitized solar cells. *Chemical reviews* **2010,** 110, (11), 6595-6663.

4. Grätzel, M., Solar energy conversion by dye-sensitized photovoltaic cells. *Inorganic chemistry* **2005,** 44, (20), 6841-6851.

5. Augustin J. McEvoy, M. G., Sustainable Energy Technologies. *Photovoltaic Cells for Sustainable Energy* **2008**, 99-119.

6. Hagfeldt, A., Brief overview of dye-sensitized solar cells. *Ambio* **2012,** 41 Suppl 2, 151-155.

7. Willinger, K.; Thelakkat, M., Photosensitizers in Solar Energy Conversion. *Photosensitizers in Medicine* **2012**, 527-617.

8. Andrade, L. M. M., *Study and characterization of Grätzel solar cells*. [s. n.]: Porto, 2010; p XXVIII, 247.

9. Sastrawan, R.; Beier, J.; Belledin, U.; Hemming, S.; Hinsch, A.; Kern, R.; Vetter, C.; Petrat, F. M.; Prodi-Schwab, A.; Lechner, P.; Hoffmann, W., New interdigital design for large area dye solar modules using a lead-free glass frit sealing. *Progress in Photovoltaics: Research and Applications* **2006,** 14.

10. Sastrawan, R.; Beier, J.; Belledin, U.; Hemming, S.; Hinsch, A.; Kern, R.; Vetter, C.; Petrat, F. M.; Prodi-Schwab, A.; Lechner, P.; Hoffmann, W., A glass frit-sealed dye solar cell module with integrated series connections. *Solar Energy Materials and Solar Cells* **2006,** 90, (11), 1680-1691.

11. Becquerel, A. E., Mémoire sur les effets électriques produits sous l'influence des rayons solaires. *Comptes Rendus des Séances Hebdomadaires* **1839,** 9, 561-567.

12. Adolf Goetzberger, J. L., Gerhard Willeke, Solar Cells: past, present an future. *Elsevier* **2002,** 74, 1-11.

13. Green, M. A., Photovoltaic Principles. *Physica E: Low-dimensional Systems and Nanostructures* **2002,** 14, (1-2), 11-17.

14. Adams, W. G.; Day, R. E., The Action of Light on Selenium. *Proceedings of the Royal Society of London Series* **1876,** 25, 113-117.

15. Fritts, C. E. In *On a New Form of Selenium Photocell*, Proceedings of the American Association for the Advancement of Science, 1883; 1883; p 97.

16. Chapin, D. M.; Fuller, C. S.; Pearson, G. L., A New Silicon p-n Junction Photocell for Converting Solar Radiation into Electrical Power. *Journal of Applied Physics* **1954,** 25, (5), 676-677.

17. Pearson, G. L., Conversion of Solar to Electrical Energy. *American Journal of Physics* **1957,** 25, (9), 591-598.

18. Fischer, H., Physics and technology of photovoltaic solar energy conversion. In *Festkörperprobleme 14*, Queisser, H. J., Ed. Springer Berlin Heidelberg: 1974; Vol. 14, pp 153-182.

19. Pinkse, J.; van den Buuse, D., The development and commercialization of solar PV technology in the oil industry. *Energy Policy* **2012,** 40, (0), 11-20.

20. Grätzel, M., Photoelectrochemical cells. *Nature* **2001,** 414, (6861), 338-344.

21. Green, M. A., Third generation photovoltaics: Ultra-high conversion efficiency at low cost. *Progress in Photovoltaics: Research and Applications* **2001,** 9, (2), 123-135.

22. Conibeer, G.; Green, M.; Corkish, R.; Cho, Y.; Cho, E.-C.; Jiang, C.-W.; Fangsuwannarak, T.; Pink, E.; Huang, Y.; Puzzer, T.; Trupke, T.; Richards, B.; Shalav, A.; Lin, K.-l., Silicon nanostructures for third generation photovoltaic solar cells. *Thin Solid Films* **2006,** 511–512, (0), 654-662.

23. Green, M. A., Third generation photovoltaics: solar cells for 2020 and beyond. *Physica E: Low-dimensional Systems and Nanostructures* **2002,** 14, (1–2), 65-70.

24. Miles, R. W.; Hynes, K. M.; Forbes, I., Photovoltaic solar cells: An overview of state-of-the-art cell development and environmental issues. *Progress in Crystal Growth and Characterization of Materials* **2005,** 51, (1–3), 1-42.

25. Grätzel, M., Dye-sensitized solar cells. *Elsevier* **2003,** 4, (2), 145-153.

26. Grätzel, M., Conversion of sunlight to electric power by nanocrystalline dye-sensitized solar cells. *Elsevier* **2004,** 164, 3-14.

27. Park, N. G.; van de Lagemaat, J.; Frank, A. J., Comparison of Dye-Sensitized Rutile- and Anatase-Based TiO2 Solar Cells. *The Journal of Physical Chemistry B* **2000,** 104, (38), 8989-8994.

28. Nazeeruddin, M. K.; Baranoff, E.; Grätzel, M., Dye-sensitized solar cells: A brief overview. *Solar Energy* **2011,** 85, (6), 1172-1178.

29. Pan, M.; Huang, N.; Zhao, X.; Fu, J.; Zhong, X., Enhanced Efficiency of Dye-Sensitized Solar Cell by High Surface Area Anatase-TiO2-Modified P25 Paste. *Journal of Nanomaterials* **2013,** 2013, 6.

30. Karmakar, A. S.; Ruparelia, J. P., A Critical Review on Dye Sensitized Solar Cells.

31. Linsebigler, A. L.; Lu, G.; Yates, J. T., Photocatalysis on TiO2 Surfaces: Principles, Mechanisms, and Selected Results. *Chemical Reviews* **1995,** 95, (3), 735-758.

32. Chen, X.; Mao, S. S., Titanium Dioxide Nanomaterials: Synthesis, Properties,Modifications, and Applications. *Journal Name: Chemical Reviews; Journal Volume: 107; Related Information: Journal Publication Date: 2007* **2007**, Medium: X.

33. Gong, J.; Liang, J.; Sumathy, K., Review on dye-sensitized solar cells (DSSCs): Fundamental concepts and novel materials. *Renewable and Sustainable Energy Reviews* **2012,** 16, (8), 5848-5860.

34. Kalyanasundaram, K.; Graetzel, M., Artificial photosynthesis: biomimetic approaches to solar energy conversion and storage. *Current Opinion in Biotechnology* **2010,** 21, (3), 298-310.

35. Peng, Y. a. Q., Review Article: Ruthenium Sensitizers and Their Applications in Dye-Sensitized Solar Cells. *International Journal of Photoenergy* **2012**, 21.

36. Yanagida, S.; Yu, Y.; Manseki, K., Iodine/Iodide-Free Dye-Sensitized Solar Cells. *Accounts of Chemical Research* **2009,** 42, (11), 1827-1838.

37. Nazeeruddin, M. K.; De Angelis, F.; Fantacci, S.; Selloni, A.; Viscardi, G.; Liska, P.; Ito, S.; Takeru, B.; Grätzel, M., Combined Experimental and DFT-TDDFT

Computational Study of Photoelectrochemical Cell Ruthenium Sensitizers. *Journal of the American Chemical Society* **2005,** 127, (48), 16835-16847.

38. Boschloo, G.; Hagfeldt, A., Characteristics of the Iodide/Triiodide Redox Mediator in Dye-Sensitized Solar Cells. *Accounts of Chemical Research* **2009,** 42, (11), 1819-1826.

39. Yu, Z.; Vlachopoulos, N.; Gorlov, M.; Kloo, L., Liquid electrolytes for dye-sensitized solar cells. *Dalton Transactions* **2011,** 40, (40), 10289-10303.

40. Brennan, L. J.; Barwich, S.; Satti, A.; Gunko, Y., Graphene - ionic liquid electrolytes for dye sensitised solar cells. *Journal of Materials Chemistry A* **2013**.

41. Brian, E. H.; Henry, J. S.; Michael, D. M., The renaissance of dye-sensitized solar cells. *Nature Photonics* **2012,** 6, (3), 162-169.

42. Chuan-Pei Lee, P.-Y. C. a. K.-C. H., *Ionic Liquid Based Electrolytes for Dye-Sensitized Solar Cells*. 2011.

43. Lee, C.-P.; Chu, T.-C.; Chang, L.-Y.; Lin, J.-J.; Ho, K.-C., *Solid-State Ionic Liquid Based Electrolytes for Dye-Sensitized Solar Cells*. 2013.

44. Yella, A.; Lee, H.; Tsao, H. N.; Yi, C.; Chandiran, A. K.; Nazeeruddin, M. K.; Diau, E. W.; Yeh, C.; Zakeeruddin, S. M.; Grätzel, M., Porphyrin-sensitized solar cells with cobalt (II/III)-based redox electrolyte exceed 12 percent efficiency. *Science* **2011,** 334, (6056), 629-34.

45. Imoto, K.; Takahashi, K.; Yamaguchi, T.; Komura, T.; Nakamura, J.-i.; Murata, K., High-performance carbon counter electrode for dye-sensitized solar cells. *Solar Energy Materials and Solar Cells* **2003,** 79, (4), 459-469.

46. Zhang, T.-L.; Chen, H.-Y.; Su, C.-Y.; Kuang, D.-B., A novel TCO- and Pt-free counter electrode for high efficiency dye-sensitized solar cells. *Journal of Materials Chemistry A* **2013,** 1, (5), 1724-1730.

47. Li, G.-r.; Wang, F.; Jiang, Q.-w.; Gao, X.-p.; Shen, P.-w., Carbon Nanotubes with Titanium Nitride as a Low-Cost Counter-Electrode Material for Dye-Sensitized Solar Cells. *Angewandte Chemie International Edition* **2010,** 49, (21), 3653-3656.

48. Roy-Mayhew, J. D.; Bozym, D. J.; Punckt, C.; Aksay, I. A., Functionalized Graphene as a Catalytic Counter Electrode in Dye-Sensitized Solar Cells. *ACS Nano* **2010,** 4, (10), 6203-6211.

49. Choi, H.; Kim, H.; Hwang, S.; Choi, W.; Jeon, M., Dye-sensitized solar cells using graphene-based carbon nano composite as counter electrode. *Solar Energy Materials and Solar Cells* **2011,** 95, (1), 323-325.

50. Cruz, R.; Pacheco Tanaka, D. A.; Mendes, A., Reduced graphene oxide films as transparent counter-electrodes for dye-sensitized solar cells. *Solar Energy* **2012,** 86, (2), 716-724.

51. J.M, K. S. W., Rhee, Electrochemical properties of porous carbon black layer as an electron injector into iodide redox couple. *Electrochimica Acta* **2012,** 83, (November 30, 2012), p. 264-270.

52. Sun, H.; Luo, Y.; Zhang, Y.; Li, D.; Yu, Z.; Li, K.; Meng, Q., In Situ Preparation of a Flexible Polyaniline/Carbon Composite Counter Electrode and Its Application in Dye-Sensitized Solar Cells. *The Journal of Physical Chemistry C* **2010,** 114, (26), 11673-11679.

53. Xiao, Y.; Wu, J.; Lin, J.-Y.; Yue, G.; Lin, J.; Huang, M.; Lan, Z.; Fan, L., A dual function of high performance counter-electrode for stable quasi-solid-state dye-sensitized solar cells. *Journal of Power Sources* **2013,** 241, (0), 373-378.

54. Ribeiro, F.; Maçaira, J.; Cruz, R.; Gabriel, J.; Andrade, L.; Mendes, A., Laser assisted glass frit sealing of dye-sensitized solar cells. *Solar Energy Materials and Solar Cells* **2012,** 96, (0), 43-49.

55. Cruz, R.; da Cruz Ranita, J. A.; Macaira, J.; Ribeiro, F.; da Silva, A. M. B.; Oliveira, J. M.; Fernandes, M. H. F. V.; Ribeiro, H. A.; Mendes, J. G.; Mendes, A., Glass–Glass Laser-Assisted Glass Frit Bonding. *Components, Packaging and Manufacturing Technology, IEEE Transactions on* **2012,** 2, (12), 1949-1956.